Investigation of the nonlinear absorption of [M(Et_2timdt)$_2$] (M = Pd, Pt) in the pico- and nanosecond timescales using the Z-scan technique

2006 J. Phys.: Condens. Matter 18 5279

(http://iopscience.iop.org/0953-8984/18/23/002)

INSTITUTE OF PHYSICS PUBLISHING JOURNAL OF PHYSICS: CONDENSED MATTER

J. Phys.: Condens. Matter **18** (2006) 5279–5290 doi:10.1088/0953-8984/18/23/002

Investigation of the nonlinear absorption of $[M(Et_2timdt)_2]$ (M = Pd, Pt) in the pico- and nanosecond timescales using the Z-scan technique

T Cassano[1], R Tommasi[2], M Arca[3] and F A Devillanova[3]

[1] Department of Physics and CNR-INFM, University of Bari, Via Amendola 173, 70126 Bari, Italy
[2] Department of Medical Biochemistry, Biology, and Physics, University of Bari, Piazza G. Cesare 11, 70124 Bari, Italy
[3] Dipartimento di Chimica Inorganica ed Analitica, S.S. 554 Bivio per Sestu, 09042 Monserrato-Cagliari, Italy

E-mail: cassano@fisica.uniba.it

Received 19 January 2006
Published 26 May 2006
Online at stacks.iop.org/JPhysCM/18/5279

Abstract

The nonlinear optical absorption of two neutral metal dithiolenes $[M(Et_2timdt)_2]$ (M = Pd and Pt) has been investigated at $\lambda = 1064$ nm by the open-aperture Z-scan technique using nanosecond and picosecond pulses. For picosecond photoexcitation, both dithiolenes mainly exhibit saturable absorption. Conversely, using nanosecond pulses, a switch from saturable absorption to reverse saturable absorption has been observed depending on the central metal. Based on experimental results, energy-level structures are suggested to explain the nonlinear absorption for both temporal regimes and, in particular, the sign-reversal of nonlinear absorption.

1. Introduction

The fields of laser technology, telecommunications, data storage, and optical switches require the development of new and efficient materials suitable for specific purposes [1]. In particular, nonlinear optical (NLO) materials have a wide range of potential applications, especially for controlling light intensity, and saturable absorption (SA), reverse saturable absorption (RSA) and two-photon absorption (TPA) [2] are among the most investigated phenomena. Today, several organic and inorganic materials are used in the NLO field, but many still suffer from some different drawbacks. For example, most of them experience laser irradiation damage depending either on the pulse intensity or on the time duration of laser irradiation, thus requiring frequent system maintenance. The class of neutral metal dithiolenes $[M(R, R'timdt)_2]$ (M = Ni, Pd, Pt; R, R′timdt = monoreduced form of disubstituted imidazolidine-2,4,5-trithione) [3] with a very high degree of π-electron delocalization extended over the whole molecule has been reported to be remarkably stable under laser excitation. The main feature

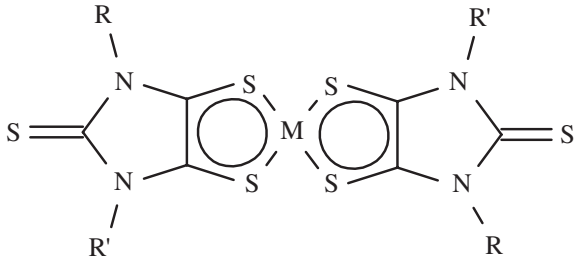

Figure 1. [M(R, R′timdt)$_2$] metal dithiolene. In sample **1**, M = Pd; in sample **2**, M = Pt. For both samples, R = R′ = C_2H_5–.

of these planar compounds has been shown to be an unusually intense near-infrared (NIR) absorption. Moreover, the changes in the metal ion and/or R and R′ substituents have allowed us to tune the spectral position of the absorption maximum λ_{max} in the range between 990 and 1032 nm [4], the absorption at the longer wavelength being obtained in chlorinated solvents when R = R′ = aromatic substituents and M = Pd. The nonlinear absorption (NLA) of these dithiolenes has previously been studied by performing pump–probe measurements with a picosecond excitation laser source. In particular, the dithiolenes with ethyl substituents and M = Pt revealed a peculiar behaviour at short time delay [5], which stimulated further investigation of the two complexes having ethyl substituents to single out the origin of the observed temporal dynamics.

In this paper, we report on the study of the NLA of two dithiolene samples differing only in the central metal ion using the open-aperture Z-scan technique and two different Nd:YAG laser sources at 1064 nm emitting 35 ps and 8 ns pulses, respectively. We will thus concentrate on the analysis of the time-integrated NLO response of the two samples under different pulse length excitations. The mechanisms leading to the observed results will be tentatively explained using multi-level rate equations.

2. Experimental details

2.1. Samples

A molecular scheme of dithiolenes belonging to the [M(R, R′timdt)$_2$] class is reported in figure 1. Numerous neutral Ni-, Pd- and Pt-dithiolenes have been prepared in the past, by changing the R and R′ substituents with a double aim: to enhance the solubility in organic solvents and, even more importantly, to tune the wavelength of the absorption maximum in the NIR region. The changes of central metal and of the substituents, together with the solvatochromic effect of the organic solvent, allowed us, for example, to obtain dithiolenes matching exactly the emission wavelengths of the Nd:YAG (λ = 1064 nm) and Nd:YLF (λ = 1053 nm) lasers [3]. The samples used in the present investigation, whose syntheses have been reported previously [3, 4], differ in the central metal ion (M = Pd for sample **1** and M = Pt for sample **2**) but bear the same substituents R = R′ = C_2H_5–. These samples, as like all other dithiolenes of the [M(R, R′timdt)$_2$] class, exhibit high extinction coefficients at wavelengths near the fundamental emission of the Nd:YAG laser (λ = 1064 nm), as can be seen in figure 2.

2.2. Z-scan

To investigate the NLA of dithiolenes, the open-aperture Z-scan technique [6] has been employed. The transmittance of a focused laser beam is measured as a function of the sample

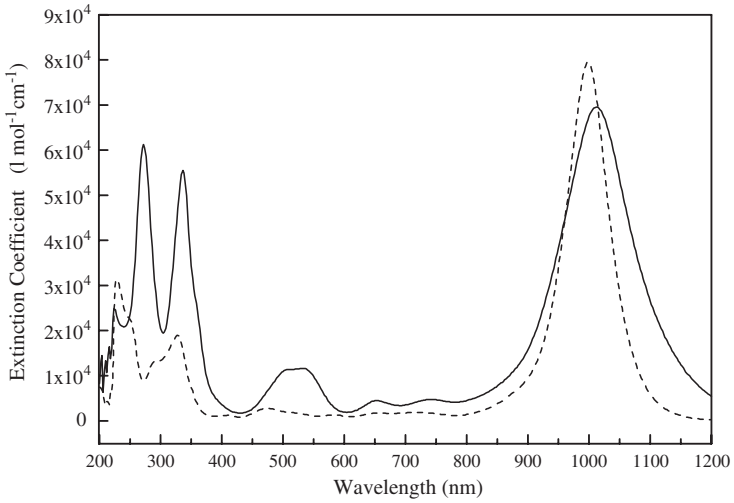

Figure 2. UV–vis–NIR linear absorption spectra of dilute solutions of sample **1** (solid line) and sample **2** (dashed line) in chloroform.

position along the beam axis, i.e. as a function of the excitation laser intensity, and the analysis of experimental data can provide third-order NLA coefficients. Usually, the Z-scan technique is used to study two-photon absorption processes, but excited-state absorption and/or absorption saturation are also detectable. To investigate the dependence of NLA on the pulse duration, two different lasers have been employed. The sources are Q-switched ($\tau \sim 8$ ns) and Q-switched and mode-locked ($\tau \sim 35$ ps) Nd:YAG lasers emitting $\lambda = 1064$ nm pulses at a repetition rate of 10 Hz, respectively. The temporal profiles of the pulses are nearly Gaussian and their spatial modes are close to TEM_{00}. Experiments have been performed at room temperature on chloroform ($CHCl_3$) solutions of the complexes, which were contained in a 1 mm thick quartz cell mounted on a 50 mm motor-driven translation stage. A $f = 10$ cm lens was used to focus the laser beams onto the cell, with a measured beam waist of (21 ± 2) μm for both lasers. For both complexes, saturated solutions were filtered and the resulting concentrations, C, were evaluated by absorbance measurements ($C_1 = 0.5 \times 10^{-4}$ M l^{-1}; $C_2 = 1 \times 10^{-4}$ M l^{-1}).

3. Results and discussion

Although our dithiolenes can be dissolved in many chlorinated solvents, the choice of $CHCl_3$ as solvent was recommended by its intrinsically low NLO coefficients. In fact, Z-scan measurements on pure $CHCl_3$ confirmed that the chloroform contribution to the measured nonlinearity of the solution can be disregarded. As experiments have been performed in a region of strong linear absorption of the dithiolenes, the main contribution to the optical nonlinearity is expected to be absorption saturation. However, other mechanisms could be present and, to distinguish among the different processes that could potentially be involved, an intensity-dependent investigation has been carried out. The power density range has been determined by setting the value of I_0 at which the nonlinear signal is detectable as the lower limit, and the maximum intensity for which a reliable signal can be measured as the upper limit. Open-aperture measurements using picosecond pulses at different excitation intensities are reported in figure 3 for the two samples. Measurements on sample **1** have been performed by varying the maximum excitation intensity I_0 over three orders of magnitude in the range 150 MW cm^{-2}–150 GW cm^{-2}. At low

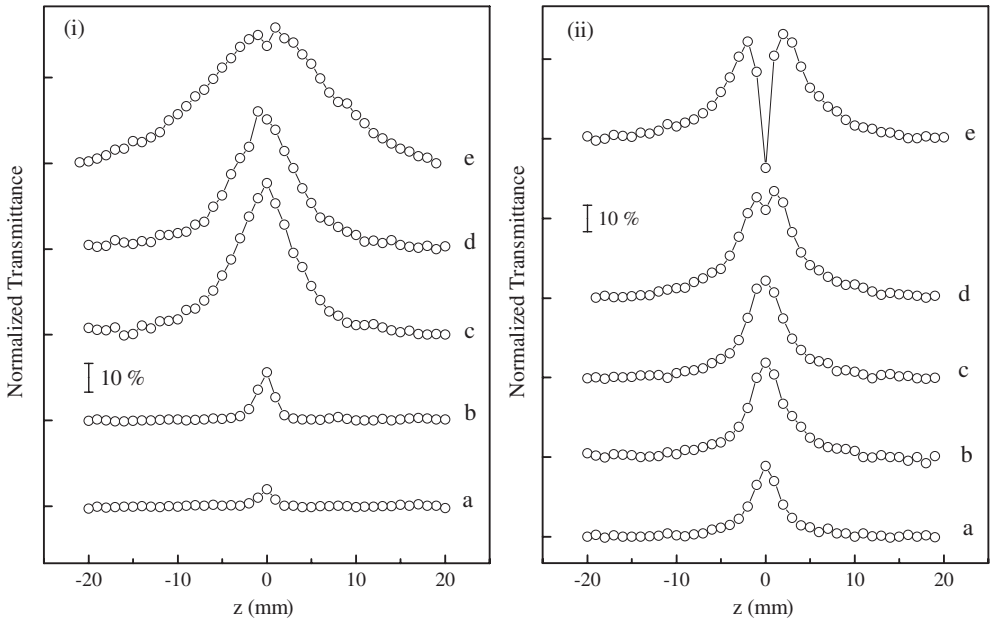

Figure 3. (i) Picosecond open-aperture Z-scan measurements on sample **1** ((a) $I_0 = 150$ MW cm^{-2}; (b) $I_0 = 450$ MW cm^{-2}; (c) $I_0 = 19$ GW cm^{-2}; (d) $I_0 = 24$ GW cm^{-2}; (e) $I_0 = 152$ GW cm^{-2}). (ii) The same for sample **2** ((a) $I_0 = 21$ GW cm^{-2}; (b) $I_0 = 35$ GW cm^{-2}; (c) $I_0 = 70$ GW cm^{-2}; (d) $I_0 = 100$ GW cm^{-2}; (e) $I_0 = 200$ GW cm^{-2}). The curves have been shifted for clarity, and the vertical bar represents the scale of normalized transmittance.

I_0 (curves **a**, **b**), an increase in transmittance with respect to the linear regime is observed by increasing the excitation intensity. By further increasing I_0, the amplitude of the transmittance peak continues to rise with approximately a linear trend until $I_0 \sim 30$ GW cm^{-2} (curve **d**). For higher intensities, the open-aperture Z-scan curves broaden, as indicated by a lower value of the ratio between the peak amplitude and the full width at half the maximum, and eventually a small dip appears close to $z = 0$ (curve **e**). This suggests that additional mechanisms, such as excited state absorption, contribute to the sample nonlinear behaviour.

As regards sample **2**, measurements have been performed between $I_0 \sim 7$ GW cm^{-2} and $I_0 \sim 200$ GW cm^{-2}. Even for sample **2** peak transmittance grows almost linearly up to $I_0 \sim 40$ GW cm^{-2}, then first the increase of the peak amplitude saturates and afterward a relative dip appears in the Z-scan curves, showing the onset of induced photo-absorption. The samples under investigation have shown superior photostability under picosecond laser irradiation with respect to other organic and inorganic complexes, which provides the opportunity of carrying experiments at very high excitation intensities. However, for $I_0 > 200$ GW cm^{-2}, measurements are not reproducible, indicating the onset of degenerative processes in the sample.

The overall behaviour of both samples for picosecond excitation pulses is thus very similar, although each shows its own peculiarities. The main feature that can be recognized is that, at relatively low excitation intensities, the absorption coefficient decreases with increasing power density. This is characteristic of saturable absorption and can be due to different mechanisms involving transitions between the ground state and excited states belonging to the singlet and/or triplet manifold. Although both samples show dominant absorption saturation, the bleaching onset takes place at much lower intensity for sample **1**.

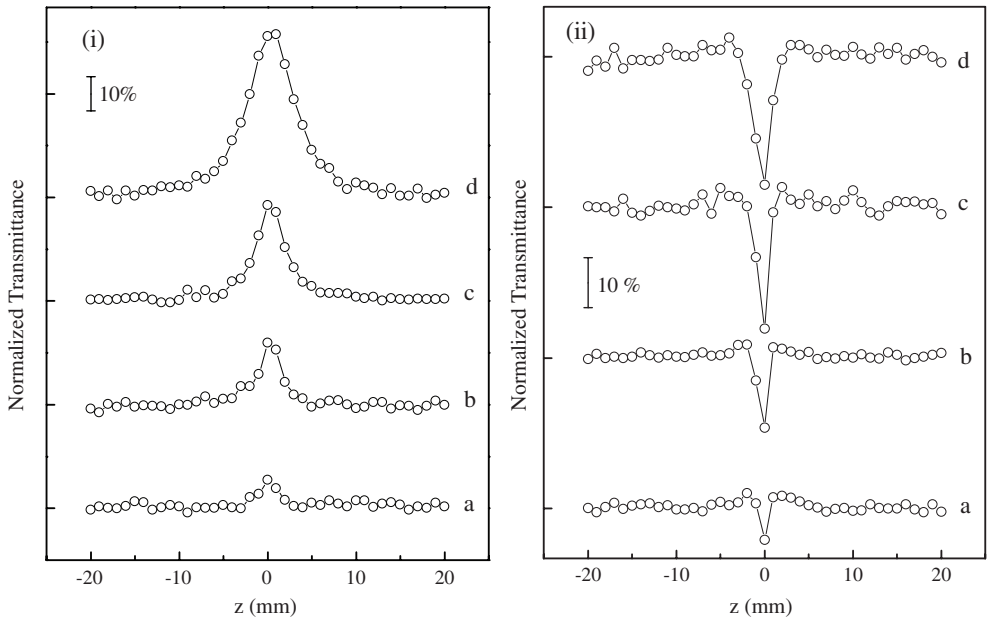

Figure 4. (i) Nanosecond open-aperture Z-scan measurements on sample **1** ((a) $I_0 = 75$ MW cm^{-2}; (b) $I_0 = 227$ MW cm^{-2}; (c) $I_0 = 590$ MW cm^{-2}; (d) $I_0 = 2.2$ GW cm^{-2}). (ii) The same for sample **2** ((a) $I_0 = 670$ MW cm^{-2}; (b) $I_0 = 1.3$ GW cm^{-2}; (c) $I_0 = 2.1$ GW cm^{-2}; (d) $I_0 = 4.4$ GW cm^{-2}). The curves have been shifted for clarity, and the vertical bar represents the scale of normalized transmittance.

Z-scan open-aperture measurements have been repeated on fresh solutions of the two samples using a laser emitting 8 ns pulses (figure 4). In this case, the onset of both the nonlinearities and degenerative molecular processes are observed at much lower power densities. Comparing the excitation densities used for the two samples, it is evident that for nanosecond photoexcitation too, the beginning of nonlinear processes takes place at higher intensity for sample **2**, following the same trend observed for picosecond measurements. For sample **1**, measurements are performed for I_0 ranging between 75 MW cm^{-2} and 2.2 GW cm^{-2} and the nonlinear mechanism is similar to the one observed for picosecond pulses. For sample **2** measurements, which have been carried out by varying I_0 between 670 MW cm^{-2} and 4.4 GW cm^{-2}, a new and unexpected nonlinear behaviour is shown. In fact, in this case, from the beginning the dominant effect is induced photo-absorption whose magnitude increases with increasing intensities. The complexity of the overall results that were obtained suggests the presence of excited-state absorption. Indeed, the decrease in transmittance with respect to the linear behaviour observed in sample **2** with nanosecond pulses could be ascribed to RSA which takes place when a particular combination of decay times and of the ratios between excited-state absorption cross sections and the fundamental absorption cross section occurs. In addition, the remarkable dependence of measurements on the pulse duration for samples **1**–**2** could be due to the involvement of triplet states through intersystem-crossing (ISC), which usually takes place on nanosecond timescales.

The experimental results are very interesting, in particular for sample **2**, for which it is sufficient to change the duration of the laser pulse to give rise to distinct and, in some regards, opposite behaviours. Indeed, for picosecond pulses, an increase in the excitation intensity induces a decrease in the sample absorption coefficient; on the contrary, for nanosecond pulses, the increase in the excitation intensity determines an enhancement of the absorption coefficient.

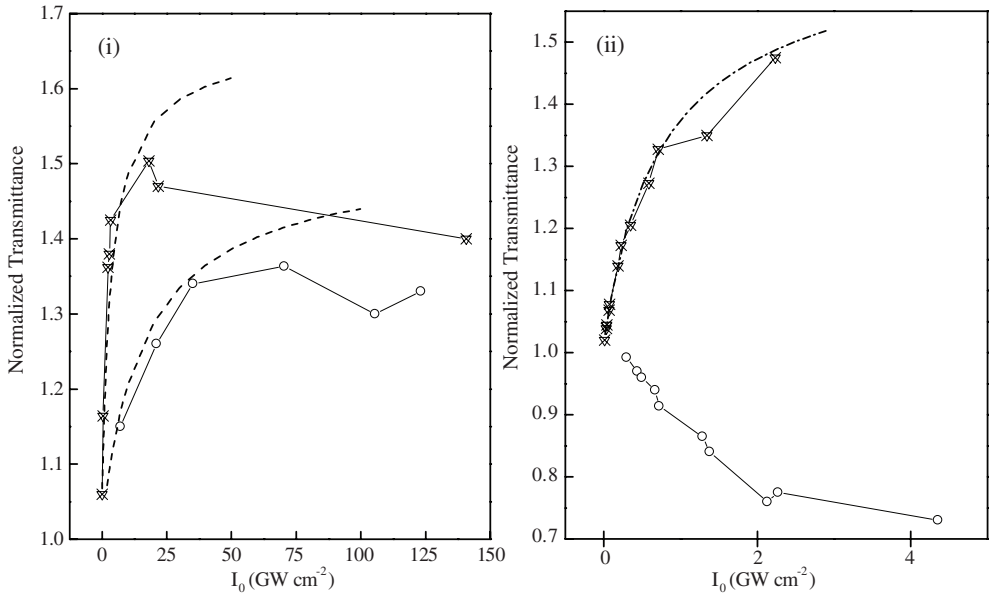

Figure 5. (i) Experimental normalized transmittance at $z = 0$ reported versus the excitation intensity for sample **1** (○) and sample **2** (⊗) obtained with 35 ps laser pulses. Dashed lines are theoretical simulations obtained using a 4-level model. (ii) Same as (i) obtained with 8 ns pulses. Dash–dot line is a theoretical simulation obtained using a 5-level model.

In what follows, we will try to outline an energy-level model suitable for describing the optical response of the investigated molecules by following the procedure reported in [7]. The normalized transmittance measured at the focus ($z = 0$) has been plotted versus I_0 for each sample for the two laser sources (figure 5). Different models were considered with the appropriate rate equations, which have been solved using a numerical procedure based on the Runge–Kutta method. As the task was to calculate the irradiance at various time, radius, and space values, the laser pulse was split into time (dt) and radius (dr) increments, while the sample was divided into space (dz) slices. Each irradiance slice was considered to experience the boundary conditions determined by the previous time slice, which enabled the solution to be obtained iteratively.

Data analysis was first performed on picosecond measurements by taking into account a simple model consisting of four singlet manifolds (figure 6), the ground state and three excited states, also including vibrational and rotational levels. Actually, a three-level model was also first considered, but the results were not satisfying at all, indicating the need to take into account an additional level. A fundamental hypothesis, which will always be assumed to be valid in what follows, is that the picosecond pulse duration is much longer than the intraband relaxation of the excited states, but much shorter than the interband time constant from the first excited state to the ground state [8]. In this case, the recovery time τ_{21} can be considered to be infinite and the relaxation from the first excited state (S_2) to the ground state can be neglected. Also, ISC has been disregarded for these measurements because it takes place on much longer timescales ($\sim 10^{-9}$ s) with respect to the pulse duration [9]. The population dynamics can be described through the following rate equations, where N_i denotes the molecular population density of the ith manifold, σ_g the fundamental absorption cross-section, σ_{23} the absorption cross-section of the transition from the first to the second excited

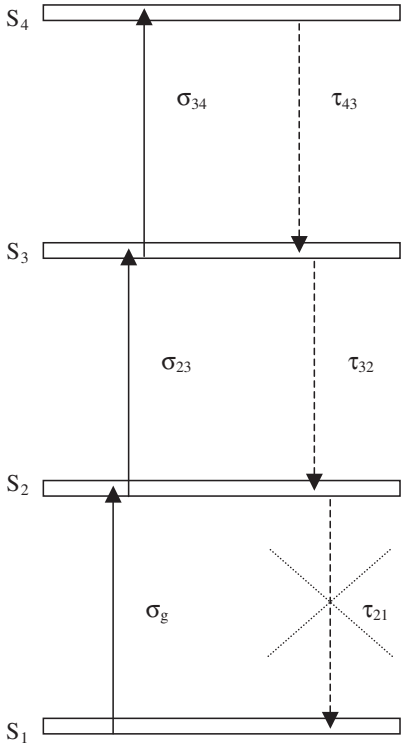

Figure 6. Scheme of the four-singlet energy-level model employed to reproduce picosecond measurements.

state, and τ_{32} the corresponding relaxation time due to spontaneous emission.

$$\begin{aligned}
\frac{\mathrm{d}N_1(t)}{\mathrm{d}t} &= -\frac{\sigma_g N_1(t) I(t)}{\hbar\omega} \\
\frac{\mathrm{d}N_2(t)}{\mathrm{d}t} &= \frac{\sigma_g N_1(t) I(t)}{\hbar\omega} - \frac{\sigma_{23} N_2(t) I(t)}{\hbar\omega} + \frac{N_3(t)}{\tau_{32}} \\
\frac{\mathrm{d}N_3(t)}{\mathrm{d}t} &= \frac{\sigma_{23} N_2(t) I(t)}{\hbar\omega} - \frac{\sigma_{34} N_3(t) I(t)}{\hbar\omega} - \frac{N_3(t)}{\tau_{32}} + \frac{N_4(t)}{\tau_{43}} \\
\frac{\mathrm{d}N_4(t)}{\mathrm{d}t} &= \frac{\sigma_{34} N_3(t) I(t)}{\hbar\omega} - \frac{N_4(t)}{\tau_{43}} \\
N_T &= N_1 + N_2 + N_3 + N_4.
\end{aligned} \tag{1}$$

The spatial pulse evolution inside the sample is determined through the following propagation equation, once the population densities have been obtained:

$$\frac{\partial I}{\partial z} = -I\left(\sigma_g N_1 + \sigma_{23} N_2 + \sigma_{34} N_3\right). \tag{2}$$

One can expect either SA or RSA to occur, depending on the magnitude of the decay times of the excited states, and on the ratios σ_{ij}/σ_g with $1 < i < j$. In figure 5, the results that are obtained are reported for both samples, showing significant agreement with experimental data only at relatively low excitation intensities ($I_0 < 18$ GW cm^{-2} for sample **1** and $I_0 < 35$ GW cm^{-2} for sample **2**). It is evident that the model is not applicable at high intensities, whilst for relatively low power densities it gives good results. However, it is crucial to test

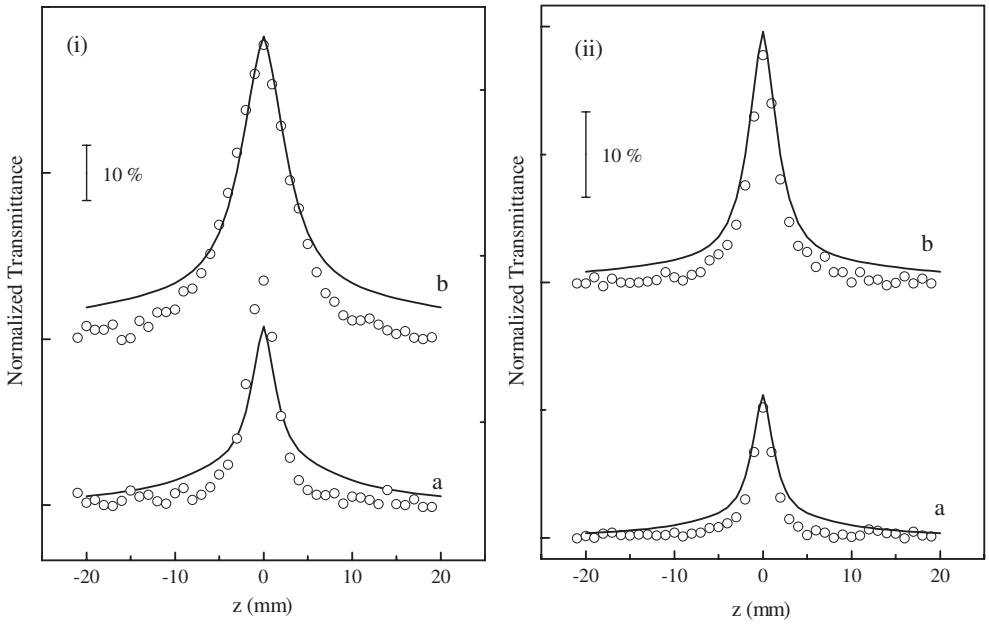

Figure 7. (i) Simulation (solid line) of the open-aperture Z-scan data (open circles) obtained using the parameters resulting from the fitting procedure of data in figure 5 for sample **1** and ps-pulses (a: $I_0 = 3$ GW cm^{-2}; b: $I_0 = 18$ GW cm^{-2}). (ii) The same for sample **2** (a: $I_0 = 7$ GW cm^{-2}; b: $I_0 = 21$ GW cm^{-2}).

the reliability of the model in the low-energy limit. This can be done by using the parameters obtained by the simulation of data in figure 5 to reproduce open-aperture Z-scan measurements at fixed excitation intensity, as one should be able to reproduce the whole Z-scan measurements using the set of parameters obtained for the transmittance at the focus position. For sample **1**, the results are reported in figure 7(i), which shows that these parameters allow rather good reproduction of the experimental results.

In fact, the overall trend (saturable absorption) of the experimental data is reproduced, although at low intensity there is no complete agreement between theory and experiments. This comparison has also been repeated for sample **2** (figure 7(ii)), giving the same qualitative indications with an even better quantitative agreement between experimental and theoretical data. In table 1, the parameters obtained using the simulation procedure are reported, showing that, even if measurements could suggest very important differences in the structure of the materials, the two samples actually behave in a quite similar manner. As a matter of fact, $\tau_{43} < \tau_{32}$ for both samples and the ratios between the first excited state absorption cross-section with respect to the ground state cross-section (σ_{23}/σ_g) and the corresponding ratios for the transition from level three to level four (σ_{34}/σ_g) are approximately the same in both cases. Since τ_{43} is very small, we studied the limit $\tau_{43} \to 0$, i.e. a three-level model, and obtained that, for the same values of σ_{23}/σ_g and τ_{32}, the bleaching effect is very much reduced with a transmittance at a high intensity lower than that obtained using the four-level model. Therefore, although decay from level 4 is fast, absorption from level three to level four cannot be neglected, because it contributes significantly to decreasing the carriers' population in level three. We conclude that a reduction in τ_{43} results in an overall decrease in the sample transmittance. This explains the different saturation transmittance values obtained for the two samples (figure 5(i)), with τ_{43} being different in the two cases. This also explains why, in the

Table 1. Parameters obtained using the four-level model for picosecond measurements and the five-level model for the nanosecond measurements.

Model	Sample	Pulse width	σ_g ($\times 10^{16}$ cm^2)	σ_{23} ($\times 10^{16}$ cm^2)	τ_{32} ($\times 10^{12}$ s)	—	σ_{34} ($\times 10^{16}$ cm^2)	τ_{43} ($\times 10^{12}$ s)	—	—
4-level	**1**	35 ps	1.7	1.4 ± 0.1	10 ± 1	—	1.4 ± 0.1	1 ± 0.1	—	—
4-level	**2**	35 ps	0.7	0.65 ± 0.1	10 ± 1	—	0.65 ± 0.1	0.5 ± 0.1	—	—
				σ_{23} ($\times 10^{16}$ cm^2)	τ_{32} ($\times 10^{12}$ s)	τ_{41} ($\times 10^{12}$ s)	τ_{24} ($\times 10^{12}$ s)	τ_{21} ($\times 10^{12}$ s)	σ_{45} ($\times 10^{16}$ cm^2)	τ_{54} ($\times 10^{12}$ s)
5-level	**1**	8 ns	1.7	1.4 ± 0.1	10 ± 1	10 ± 1	10 ± 1	10 ± 1	2 ± 0.2	1 ± 0.1

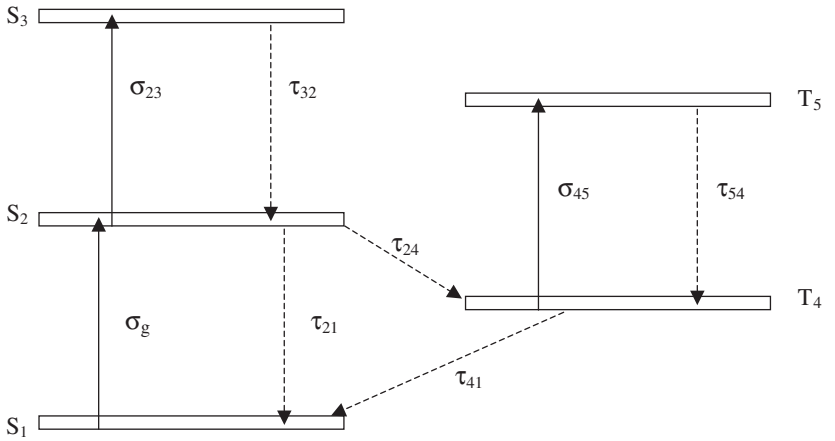

Figure 8. Scheme of the five-energy level model employed to reproduce nanosecond measurements.

two cases, there is a large variation in the lowest value of the excitation intensity I_0 at which a nonlinear process is observed. In fact, a higher value of τ_{43} determines a lower population density N_3, thus suggesting that absorption saturation between levels two and three takes place at higher intensity. To summarize, we observe that the unique differentiation in the sets of parameters obtained for the two samples is just in the value of τ_{43}, which is smaller in the case of sample **2**, as expected.

As regards nanosecond measurements, the same model used for picosecond pulses has been tested, but the results were in disagreement with the experimental results. Therefore, the level scheme was modified by adding transitions to the triplet states (figure 8) because, for nanosecond pulses, one expects ISC to be effective. We also tried to reduce the number of singlet levels involved, and the best compromise was found with three energy levels within the singlet system and two levels in the triplet system (thus giving a five-level model). Furthermore, the transition from the first excited state to the ground state could no longer be neglected, since the time duration of the excitation pulses was comparable to this decay time. For the same reason, the decay time from the first triplet state to the ground state also had to be considered. The rate equations are then:

$$\begin{aligned}
\frac{\mathrm{d}N_1(t)}{\mathrm{d}t} &= -\frac{\sigma_g N_1(t) I(t)}{\hbar\omega} + \frac{N_2(t)}{\tau_{21}} + \frac{N_4(t)}{\tau_{41}} \\
\frac{\mathrm{d}N_2(t)}{\mathrm{d}t} &= \frac{\sigma_g N_1(t) I(t)}{\hbar\omega} - \frac{\sigma_{23} N_2(t) I(t)}{\hbar\omega} + \frac{N_3(t)}{\tau_{32}} - \frac{N_2(t)}{\tau_{24}} - \frac{N_2(t)}{\tau_{21}} \\
\frac{\mathrm{d}N_3(t)}{\mathrm{d}t} &= \frac{\sigma_{23} N_2(t) I(t)}{\hbar\omega} - \frac{N_3(t)}{\tau_{32}} \\
\frac{\mathrm{d}N_4(t)}{\mathrm{d}t} &= -\frac{N_4(t)}{\tau_{41}} + \frac{N_2(t)}{\tau_{24}} - \frac{\sigma_{45} N_4(t) I(t)}{\hbar\omega} + \frac{N_5(t)}{\tau_{54}} \\
\frac{\mathrm{d}N_4(t)}{\mathrm{d}t} &= \frac{\sigma_{45} N_4(t) I(t)}{\hbar\omega} - \frac{N_5(t)}{\tau_{54}} \\
N_T &= N_1 + N_2 + N_3 + N_4 + N_5
\end{aligned} \tag{3}$$

with the spatial pulse evolution inside the sample described by

$$\frac{\partial I}{\partial z} = -I\left(\sigma_g N_1 + \sigma_{23} N_2 + \sigma_{45} N_4\right). \tag{4}$$

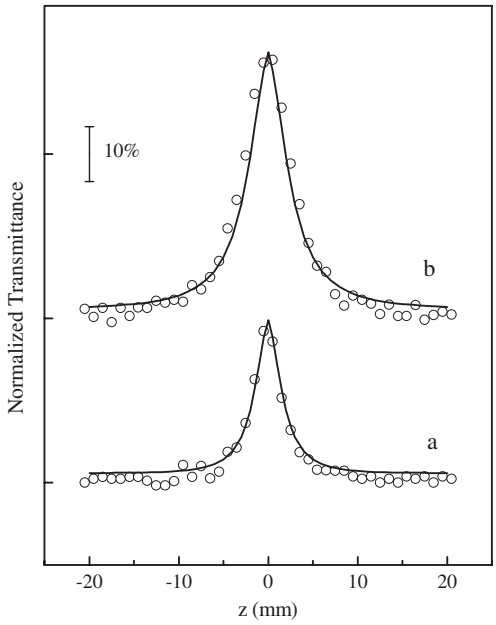

Figure 9. Simulation (solid line) of the open-aperture Z-scan data (open circles) obtained using the parameters resulting from the simulation procedure of data in figure 5 for sample **1** and ns-pulses (a: $I_0 = 600$ MW cm^{-2}; b: $I_0 = 2.3$ GW cm^{-2}).

This model was used to calculate the theoretical curve reported in figure 5(ii) for sample **1**, giving very good agreement with experimental data in the whole range of power densities considered. In figure 9, Z-scan measurements at selected intensities are reported, together with the simulation of the data performed using the simulation parameters obtained with the five-level model. Also in this case, the agreement between experimental and theoretical data is remarkable, thus confirming that the outlined model describes the energy levels involved in the present investigation very well. Conversely, as regards sample **2**, in the nanosecond regime at the moment we do not have satisfying results, although some preliminary findings give good indications of the validity of the five-level model already used for sample **1**.

4. Conclusions

In this paper, we have investigated nonlinear absorption in two neutral metal dithiolene complexes belonging to the class [M(R, R′timdt)$_2$] differing only in the central metal ion. Single-beam open-aperture Z-scan measurements have been performed on chloroform solutions at $\lambda = 1064$ nm using two different Nd:YAG laser sources emitting $\tau \sim 35$ ps and $\tau \sim 8$ ns pulses, respectively. Picosecond measurements show saturable absorption for both samples. In contrast, nanosecond measurements give saturable absorption for samples having M = Pd as the central metal ion (sample **1**) and reverse saturable absorption for the sample having M = Pt in the central position (sample **2**). This demonstrates that nonlinear optical properties of these complexes can be very sensitive to the pulse duration of the excitation source. Moreover, for both samples, picosecond measurements have been simulated by using a four-level model, obtaining reasonable results, especially at low excitation intensities. For nanosecond measurements, a five-level model involving triplet states has been considered.

Sample **1** measurements have been simulated successfully, while for sample **2** no set of parameters has been found for reproducing experimental results, thus suggesting that additional nonlinear mechanisms could be involved in the latter case. Further investigations will be addressed for sample **2**, and the results reported in a forthcoming publication.

Acknowledgments

The financial support of MIUR PRIN Project No 2003095258_002 and 2003095258_004 is gratefully acknowledged.

References

[1] Zyss J (ed) 1993 *Molecular Nonlinear Optics: Materials, Physical and Devices* (Boston, MA: Academic)
Marder S R *et al* (ed) 1991 *Materials for Nonlinear Optics—Chemical Perspectives* (*ACS Symp. Ser.*) (Washington, DC: Americal Chemical Society)
Prasad P N and Williams D J (ed) 1991 *Introduction to Nonlinear Optical Effects in Molecules and Polymers* (New York: Wiley)
Kuhn H and Rubillard J (ed) 1992 *Nonlinear Optical Materials* (Boca Raton, FL: CRC Press)
[2] Tutt L W and Boggess T F 1993 *Prog. Quantum Electron.* **17** 299
[3] Bigoli F, Deplano P, Devillanova F A, Lippolis V, Lukes P J, Mercuri M L, Pellinghelli M A and Trogu E F 1995 *J. Chem. Soc., Chem. Commun.* 371
Bigoli F, Deplano P, Devillanova F A, Ferraro J R, Lippolis V, Lukes P J, Mercuri M L, Pellinghelli M A, Trogu E F and Williams J M 1997 *Inorg. Chem.* **36** 1218
Arca M, Demartin F, Devillanova F A, Garau A, Isaia F, Lelj F, Lippolis V, Pedraglio S and Verani G 1998 *J. Chem. Soc. Dalton Trans.* 3731
[4] Aragoni M C, Arca M, Demartin F, Devillanova F A, Garau A, Isaia F, Lelj F, Lippolis V and Verani G 1999 *J. Am. Chem. Soc.* **121** 7098
[5] Cassano T, Tommasi R, Nitti L, Aragoni M C, Arca M, Denotti C, Devillanova F A, Isaia F, Lippolis V, Lelj F and Romaniello P 2003 *J. Chem. Phys.* **118** 5995
[6] Sheik-Bahae M, Said A A, Wei T-H, Hagan D J and Van Stryland E W 1990 *IEEE J. Quantum Electron.* **26** 760
[7] Cassano T, Tommasi R, Meacham A P and Ward M D 2005 *J. Chem. Phys.* **122** 154507
[8] Wei T-H and Huang 1996 *Opt. Quantum Electron.* **28** 1495
[9] Lepkowicz R, Kobyakov A, Hagan D J and Van Stryland E W 2002 *J. Opt. Soc. Am.* B **19** 94